Biointerphases (2012) 7:23
DOI 10.1007/s13758-012-0023-0

ARTICLE

Regulation of Integrin Adhesions by Varying the Density of Substrate-Bound Epidermal Growth Factor

Tamar Shahal · Benjamin Geiger · Iain E. Dunlop · Joachim P. Spatz

Received: 23 December 2011 / Accepted: 13 February 2012 / Published online: 3 March 2012

Abstract Substrates coated with specific bioactive ligands are important for tissue engineering, enabling the local presentation of extracellular stimulants at controlled positions and densities. In this study, we examined the cross-talk between integrin and epidermal growth factor (EGF) receptors following their interaction with surface-immobilized Arg-Gly-Asp (RGD) and EGF ligands, respectively. Surfaces of glass coverslips, modified with biotinylated silane-polyethylene glycol, were functionalized by either biotinylated RGD or EGF (or both) via the biotin–NeutrAvidin interaction. Fluorescent labeling of the adhering A431 epidermoid carcinoma cells for zyxin or actin indicated that EGF had a dual effect on focal adhesions (FA) and stress fibers: at low concentrations (0.1; 1 ng/ml), it stimulated their growth; whereas at higher concentrations, on surfaces with low to intermediate RGD densities, it induced their disassembly, leading to cell detachment. The EGF- dependent dissociation of FAs was, however, attenuated on higher RGD density surfaces. Simultaneous stimulation by both immobilized RGD and EGF suggest a strong synergy between integrin and EGFR signaling, in FA induction and cell spreading. A critical threshold level of EGF was required to induce significant variation in cell adhesion; beyond this critical density, the immobilized molecule had a considerably stronger effect on cell adhesion than did soluble EGF. The mechanisms underlying this synergy between the adhesion ligand and EGF are discussed.

Electronic supplementary material The online version of this article (doi:10.1007/s13758-012-0023-0) contains supplementary material, which is available to authorized users.

T. Shahal · B. Geiger (✉)
Department of Molecular Cell Biology, Weizmann Institute of Science, 76100 Rehovot, Israel
e-mail: benny.geiger@weizmann.ac.il

I. E. Dunlop
Department of Materials, Imperial College London, London SW7 2AZ, UK

J. P. Spatz
Department for New Materials and Biosystems, Max-Planck-Institute for Intelligent Systems, 70569 Stuttgart, Germany

J. P. Spatz
Department of Biophysical Chemistry, Institute for Physical Chemistry, University of Heidelberg, INF 253, 69120 Heidelberg, Germany

1 Introduction

This study focuses on the cross-talk between an adhesive (RGD) and a signaling (EGF) molecule, and its impact on cell–matrix adhesion. RGD is a known adhesion peptide, which has been introduced into cells in an immobilized form [1]. EGF is a growth factor present in a soluble form. It has been shown that the EGF receptor (EGFR) and its downstream signaling cascade are activated only when integrin receptors are aggregated and activated by their respective adhesion ligands [2]. The cross-talk between these two ligand-receptor systems also affects the reciprocal process; namely, integrin-mediated adhesion [3–5]. Thus, the addition of soluble EGF to the epidermoid carcinoma cells, A431 and other cell types resulted in the formation of aligned actin stress fibers [3, 6–8]. Live-cell imaging and electron microscopy have revealed major cytoskeletal rearrangements in EGF-treated A431 cells, manifested by extensive lamellipodia and filopodia extension, and induction of membrane ruffling [7, 9]. In some studies, growth and elongation of focal adhesions along

actin stress fibers following soluble EGF stimulation was reported in fibroblasts and other cell types [5, 10, 11]. In contrast, other studies have suggested that EGF-mediated signaling promotes structural cytoskeletal changes which lead to cell polarization, the generation of intercellular contractile forces [6], and partial disassembly of focal adhesions, that eventually promote cell migration [8].

The spatial distribution of cell-surface receptors for the extracellular matrix (ECM), as well as of a variety of growth factors, has a major influence on their activation and function. For example, cell adhesion to the matrix induces the clustering of transmembrane integrins into actin-associated focal adhesions (FA) [12, 13]. Further recruitment of multiple scaffolding and signaling "adhesome" molecules, such as vinculin, talin, zyxin and focal adhesion kinase (FAK) [14] play a central role in regulating the ECM adhesion process, as well as its subsequent regulation of cell survival, division and differentiation [14–17]. Similarly, the EGF-induced, autophosphorylation-driven clustering of epidermal growth factor receptors (EGFR), is essential for the activation of the relevant downstream signaling cascades [18–20].

The immobilization of different types of effectors' molecules to a surface has been found to be critical for controlling their effect on cell behavior. For example, an integrin-dependent spreading, polarization and migration of dendritic cells was found to be induced by immobilized but not soluble CC21 (a chemokine for CC-chemokine receptor 7) [21]. Similarly, surface-immobilized EGF has been shown to be particularly effective in inducing cell survival [22], proliferation [17, 23] and differentiation [24] of various cell types. For example, surface-tethered EGF was considerably more effective than soluble EGF in promoting mesenchymal stem cell (MSC) spreading and survival [22]; neurogenic differentiation of pheochromocytoma (PC12) cells occurred with immobilized EGF, but not with soluble growth factor. This finding relates to the long-lasting duration of the stimulation compared to that of the soluble molecules, which were degraded via receptor-mediated endocytosis [24].

In addition, this hyperactivity of surface-bound EGF raised the possibility that the EGFR might affect, and be affected by, matrix adhesion molecules such as integrins. This notion has so far attracted only scant attention; it has, however, been shown that the response of cells to soluble EGF depends on the surface densities of fibronectin and collagen, which affected the adhesion and motility of various cell types [5, 25, 26]. Recently, Elloumi et al. [27] showed that human lung carcinoma epithelial cells retained their adhesiveness and growth activity when plated on culture plates coated with a protein complex containing both RGD and EGF molecules, conjugated by a hydrophobic protein. Yet the mechanism underlying the synergy between integrins and EGFR remains largely unknown. For example, it is still unclear whether EGF affects FAs in a general manner, or whether it involves local cross-talk between the EGFR and the integrin-mediated adhesions. This issue; namely, the exact site of action of growth factor receptors, is potentially important for the fabrication of implants to be used in tissue engineering and regenerative medicine [28].

To study the mechanism underlying EGFR-integrin cooperation, we functionalized glass surfaces with biotin-NH-CH2-CH2(O-CH2-CH2)n-NHCONH(CH2)3-Si(OEt)3 (silane-PEG-biotin). This polymer contains a PEG backbone, known for its non-adhesive properties [29–32], and terminated with a biotin molecule. Biotin displays a strong affinity for avidin, streptavidin and NeutrAvidin (K_d of 10^{-15} M^{-1}), and is also highly specific [33]. Biotin-terminated PEG has previously been anchored to surfaces using a variety of chemistries, including electrostatic attachment via positively-charged lysine groups [34], the adhesive amino acid DOPA [35], and attachment to reactive self-assembled silane layers [36, 37]. The single–step silane-anchoring approach used here has been shown to produce a surface that repels most proteins, but can be functionalized with streptavidin [29]. We modified the biotin-functionalized surfaces using NeutrAvidin–biotin-modified RGD/EGF complexes at varying concentrations, thus obtaining surfaces functionalized with RGD alone, or with RGD and EGF, at different densities (schematic presentation in Fig. 1). Next, we tracked the adhesion and spreading patterns of A431 cells as a function of the relative densities of immobilized RGD and EGF. We then compared the cell adhesion response to surface-immobilized EGF, with the response to soluble EGF; namely, the response to local stimulation, at adhesion sites versus global stimulation, respectively.

We show here that EGF and RGD can exhibit either positive or negative cooperativity. Thus, EGF can act either as an adhesion enhancer or an adhesion suppressor, depending on: (a) EGF quantities, (b) RGD density, (c) mode of application, soluble or immobilized, and (d) duration of application. For example, when EGF was applied in a soluble form for 30 min, 5 h after cell plating, it behaved as an adhesion stimulator up to a certain concentration, above which it led to cell detachment. The threshold detachment concentration was dependent on the RGD density: the higher the RGD density, the higher the inhibitory threshold concentration. Moreover, on high RGD density surfaces, immobilized EGF enhanced adhesion more strongly than soluble EGF (as manifested by an increase in the number of FAs) up to 164.9 ± 42.3 pmol/cm^2 at which cell detachment was observed with immobilized EGF, but not with soluble EGF. A significant cell adhesion response was obtained at an EGF density of

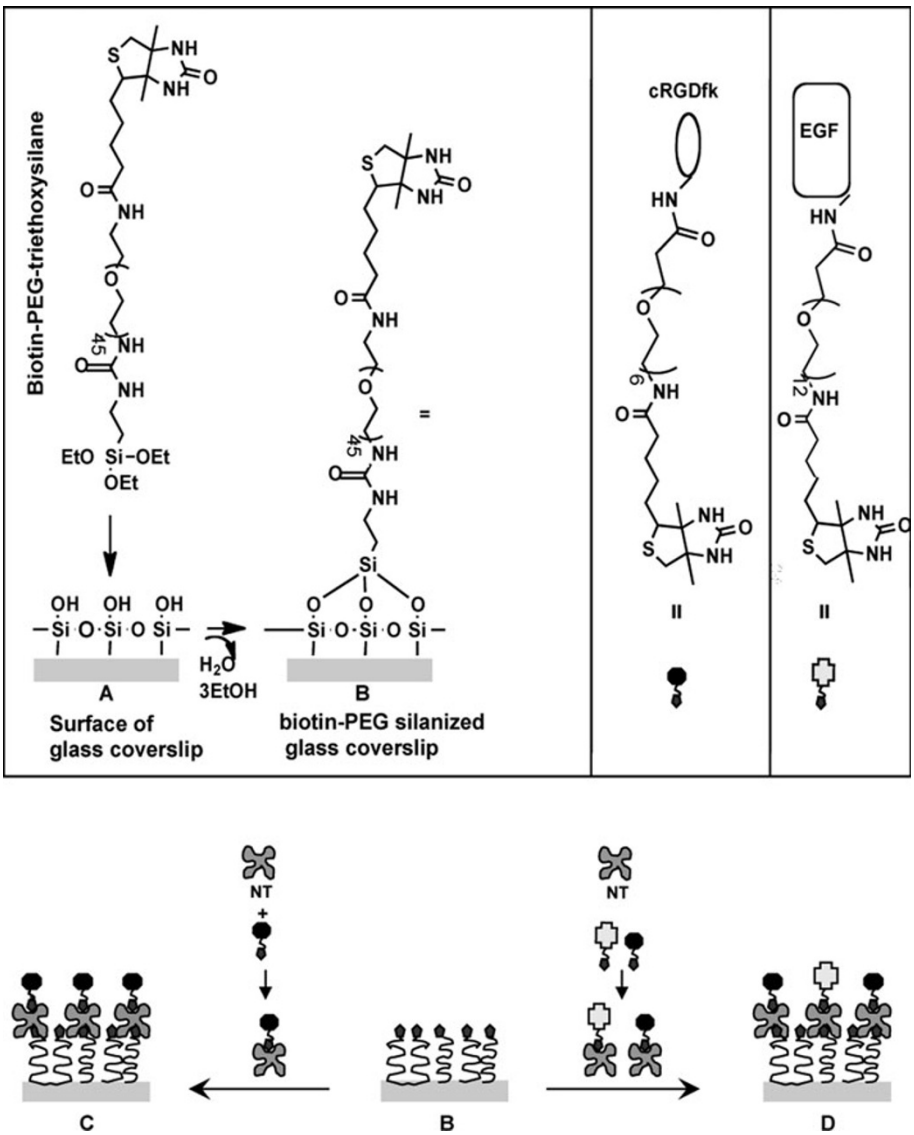

Fig. 1 A schematic presentation of RGD and EGF surface functionalization. Plasma -etched glass slides (**a**) are incubated with triethoxysilane–PEG–biotin in toluene, resulting in the formation of biotinylated glass slides (**b**). The biotinylated glass slides are further incubated with preformed NeutrAvidin (NT)–biotin–EGF/RGD complexes at various complex concentrations, resulting in the formation of glass cover slips biofunctionalized with RGD (**c**) or with a mixture of RGD and EGF at different densities and ratios (**d**)

3.8 ± 1.4 pmol/cm^2, and pronounced differences between the cellular response to global and local EGF stimulation were observed above this density. These cellular behaviors may be due to the physical proximity of the activated EGFR to RGD-anchored integrins, and the apparent synergism between these two receptor systems.

2 Experimental

2.1 Biotinylation of Proteins

The c[RGDfK] [3–5], modified at the Lys side chain by a short biotin-oligo(EG)$_6$ linker (biotin-RGD, Fig. 1), was custom-synthesized by Biosyntan, (Berlin, Germany). Biotin-conjugated murine EGF (PeproTech Inc., Rocky Hill, NJ, USA) was prepared using an amine-reactive biotin labeling reagent with a long polyethylene glycol (PEG) spacer arm (56 Å), N-hydroxysuccinimid (NHS)-CO-(O-CH_2-CH_2)$_{12}$-NHCO(CH_2)$_4$-biotin (NHS-PEG$_{12}$-biotin, Fig. 1). The N-hydroxysuccinimide ester (NHS) group reacts specifically and efficiently with primary amines found in lysine and N-terminal amino groups, to form stable amide bonds. We chose to biotinylate murine- rather than human EGF, since murine EGF does not contain lysines in its structure, and hence displays an amine-reactive group only at its N-terminus, so that the protein's activity is not affected by the biotin modification. The non-reactive biotinylation reagent was separated from the biotinylated protein using Zeba Spin Desalting columns; the protein biotinylation efficiency was determined by a Quantitation Kit. All the latter products were purchased from Thermo Fisher Scientific Pierce Biotechnology, Rockford, Illinois, USA. The effect of soluble mouse-biotin

EGF on A431 FAs was similar to that of human EGF (Figs. 3d, 5e).

2.2 Preparation of Substrates

Specifically functionalized monolayers were prepared and stored under argon, using biotin-NH-CH_2-CH_2(O-CH_2-CH_2)$_n$-NHCONH$(CH_2)_3$-Si$(OEt)_3$ (silane-PEG-biotin); ((O-CH2-CH_2)$_n$ section has Mw = 2,000 Da; Fig. 1), a custom synthesis obtained from Rapp Polymere GmbH (Tübingen, Germany) according to a procedure previously described (24). Glass coverslips 60 × 24 mm #1 (Marienfeld, Lauda- Konigshofen, Germany) were cleaned with Hellmanex 2% detergent (Hellma GmbH, Mullheim, Germany) for 45 min, then thoroughly rinsed with water, ethanol and acetone, dried at 80°C, and then treated for 5 min with air plasma in a Plasma Cleaner/Sterilizer PDC-32G (Harrick Scientific, Ossining, NY, USA). This procedure was conducted in order to remove any organic contaminants, and create hydroxyl groups on the glass surface. The plasma-treated substrates were immediately inserted into a flask connected to a stream of nitrogen. To form self-assembled monolayers, dry toluene (60 ml, >99.9% purity) (Merck KGaA, Darmstadt, Germany), dried with molecular sieves, was added to the flask containing the substrate, followed by triethylamine (Sigma-Aldrich, Seelze, Germany), milliQ water (0.1% of the toluene volume) and silane–PEG–biotin (3–5 mg). The flask was then sealed and incubated at 80°C for 12 h, after which the substrates were washed with ethyl acetate (Gadot, Herzlia, Israel) and methanol (Biolab, Jerusalem, Israel) and then dried under a stream of nitrogen. All solvents were analytical grade. The formation of pure, homogenous monolayers of silane-PEG-biotin was shown by Kartos AXIX-HS XPS (Fig. S1, Supplementary Information).

The silane–PEG–biotin-modified slides were mounted onto the bottom of a Flexiperm silicon gasket (Sastedt, Numbrecht, Germany), dividing the slide into 12 separate wells of 5 mm diameter each. NeutrAvidin (Thermo Fisher Scientific Pierce Biotechnology)–biotin–RGD/EGF complexes at a 1:2 ratio were pre-formed by incubation at room temperature. Surfaces presenting RGD or a combination of RGD and EGF, at various densities, were formed by incubating the silane–PEG–biotin glass slides with various concentrations of the NeutrAvidin–biotin–RGD complex in PBS, or a mixture of NeutrAvidin–biotin–RGD/EGF complexes in PBS for 30 min at 37°C, as indicated in the results section (Fig. 1).

The application of 0.1 mg/ml DyLight488-labeled NeutrAvidin (Thermo Fisher Scientific Pierce Biotechnology, Rockford, United States) has resulted in surface saturation with the protein (Fig. S2, Supplementary Information). The spacing between adjacent biotin groups on the silane–PEG–biotin -modified glass surface was calculated to be 4.6 nm, based on XPS measurements (Fig. S1, Supplementary Information). Since the cross-section of NeutrAvidin is about 4.5 nm, this surface density of biotin is enough to induce surface saturation with NeutrAvidin.

The density of NeutrAvidin–biotin–EGF complex bound to the biotinylated surface was determined by the gamma-irradiation of I^{125}- labeled biotin-EGF. A graph showing the density of surface- adsorbed NeutrAvidin–biotin–EGF-I^{125} as a function of the concentration of the applied solution is shown in Fig. S3, Supplementary Information. The amount of surface-immobilized NeutrAvidin–biotin–EGF complex was not significantly affected by the concentration of NeutrAvidin–biotin–RGD complex applied in the same solution, since the surface coverage was well below saturation for all concentrations used (Fig. S3, Supplementary Information). Since both RGD and EGF are much smaller than a NeutrAvidin molecule (0.9, 6.4 and 60 kDa, respectively) the surface coverage for a given solution concentration can be taken to be the same for NeutrAvidin–biotin–RGD as for NeutrAvidin–biotin–EGF. Hence, the density of NeutrAvidin–biotin–RGD was calculated from the gamma radiation of NeutrAvidin–biotin–EGF- I^{125}.

2.3 Cell Culture

A431 epidermoid carcinoma cells from the American Type Culture Collection (ATCC) (Manassas, VA, USA) were chosen due to the high number of EGF receptors expressed on their surface (3×10^6/cell). Cells were cultured in Dulbecco's modified Eagle's medium (DMEM) supplemented with 10% fetal calf serum, and regularly replated by a treatment with trypsin–EDTA solution. Tissue culture medium, fetal calf serum, trypsin–EDTA, penicillin–streptomycin and sodium pyruvate solutions were obtained from Gibco (Gibco Company, Carlsbad, CA, USA). Cells were maintained at 37°C in a humidified incubator, under 5% CO_2.

2.4 Cell Adhesion Assay

A431 cells were grown to ~70% confluence, and serum-starved for 12 h in DMEM containing 1% bovine serum albumin (BSA) fraction V (Serva Electrophoresis GmbH, Heidelberg, Germany), 1% sodium pyruvate, and 1% penicillin–streptomycin. The starved A431 cells were harvested by trypsin–EDTA, plated at a density of 7.5×10^4 cells/cm^2 in the same serum-free medium on either RGD or on both RGD- and EGF-functionalized surfaces, and incubated for 5 h, the amount of time needed for the A431 cells to adhere and fully spread on the

functionalized surfaces. Following the incubation period, cells plated on RGD functionalized surfaces were exposed to various concentrations of soluble human EGF (Sigma-Aldrich Israel, Ltd., Rehovot, Israel) for 30 min, and then fixed and stained for zyxin and actin. Cells plated on surfaces functionalized with both RGD and murine EGF were fixed and stained directly after the incubation period. To compare cellular responses to stimulation by immobilized and soluble murine biotin-EGF stimulation, equal numbers of either soluble or immobilized molecules were introduced into each well. Soluble murine biotin-EGF was added immediately after cells were plated on surfaces modified with RGD only, allowing a total of 5 h incubation with the soluble molecule.

2.5 Immunochemical Reagents and Indirect Immunofluorescence

For the staining of focal adhesions and actin filaments, cells cultured on the functionalized surfaces were fixed and permeabilized for 5 min in 3% paraformaldehyde (PFA) containing 0.5% Triton X-100 (Sigma-Aldrich Ltd., Rehovot Israel), and then further fixed with 3% paraformaldehyde in PBS for 30 min. Triple-labelling for visualization of focal adhesions, the actin cytoskeleton, and nuclei was achieved by incubating cells with zyxin primary rabbit antibodies (B71/72, kindly provided by Mary Beckele, University of Utah, [38]), and a mixture of goat anti-rabbit Cy3 (Jackson ImmunoResearch, West Grove, PA, USA), TRITC-labeled phalloidin, and DAPI (Sigma-Aldrich, St. Louis, MO, USA).

2.6 Microscopy and Image Analysis

Microscopic imaging was conducted using a WiScan automated microscope (Idea Bio-Medical, Ltd., Rehovot, Israel). Images of fluorescently-stained cells were acquired with a 60×/0.90 NA Olympus objective, Olympus Europa GmbH, Hamburg, Germany, and analyzed using Prism software. The acquired images in each well were tiled into montages, to give an overall visual impression of the cells, while still maintaining the full resolution of the individual images. Specific features of focal adhesions—FA area, FA elongation (aspect ratio), and number of FAs per cell—were calculated, as previously described by Paran et al. [39]. In brief, high-pass filtered images are first segmented, using a WaterShed threshold algorithm [40, 41], and for each FA, morphological, fluorescence-intensity, and estimated background parameters are calculated. Object-by-object, multiparameter data for each image were saved in separate files. User-controlled ranges for each parameter (kernel size for the high pass filter, minimum and maximum object size, threshold gates) defined the objects to be included in the montage, and the outliers to be excluded.

Values of the parameters characterizing cell morphology—cell elongation (aspect ratio of best-fit ellipse) and cell projection area were determined using Image J software.

2.7 Data Analysis

The statistical distribution of the morphological FA and cell parameters was not a normal Gaussian distribution and hence, the values of these parameters were primarily based on the 70th or 90th percentile values calculated for each parameter, as indicated (i.e., the parameter values below which 70 or 90% of all cells/FAs are found). Cell shape and FA parameters were measured in at least 80 individual cells for each experimental treatment. Each experiment was repeated at least three times.

3 Results and Discussion

3.1 RGD Density Affects Cell Attachment and Spreading

It was shown that integrin clustering is essential for cell-surface attachment, spreading and FA formation [12, 13]; hence, attachment and spreading of A431 epidermoid carcinoma cells were investigated on surfaces functionalized with varying RGD densities. Figure 2 shows that A431 spreading and polarization varies greatly, depending on RGD surface density. At low RGD densities (6–12 pmol/cm^2) cells attached to the surface but failed to spread, and in many cases were more elongated in shape, whereas at high RGD densities (23–184 pmol/cm^2 RGD), cells were well spread with peripheral actin bundles. A similar range of RGD density was required for the formation of cells with well-formed stress fibers on star polymers presenting RGD [26]. Surfaces modified with only silane–PEG–biotin or with silane–PEG–biotin + NeutrAvidin without biotin-RGD, were completely inert to cell adhesion.

3.2 Soluble EGF Induces FA Growth

It was previously shown that the addition of EGF to the growth medium of serum-starved cells results in a significant growth of FAs, and the associated actin stress fibers [10]. Similarly, A431 cells plated on high-density RGD or FN surfaces in serum-free medium formed only small FAs in the absence of EGF; yet application of increasing concentrations of soluble EGF resulted in a major increase in

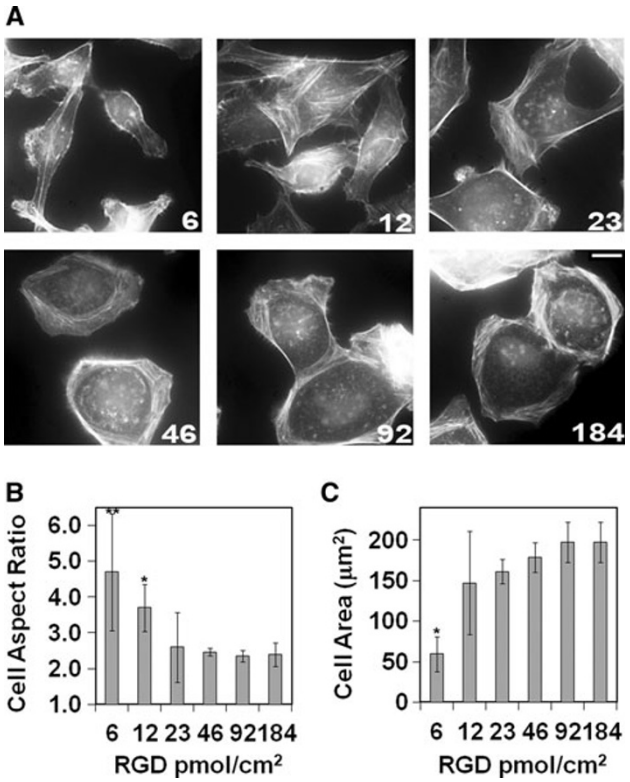

Fig. 2 A431 cell spreading on RGD-biofunctionalized surfaces at varying densities. The fluorescent images in the top panel are of actin-labeled A431 cells; the numbers on each image indicate the RGD density in pmol/cm^2 (**a**), *scale bar* 15 μm. The *graphs* in the *bottom panel* display the 90th percentiles of cell aspect ratio (**b**) and cell area (**c**). All results are expressed as mean ± confidence intervals (CI). Aspect ratio and area of cells plated on 6 and 12 pmol/cm^2 RGD surfaces that significantly differed from 46 pmol/cm^2 RGD surfaces at the *P*-value levels $P < 0.05$ and $P < 0.01$ are denoted by one and two *asterisks*, respectively

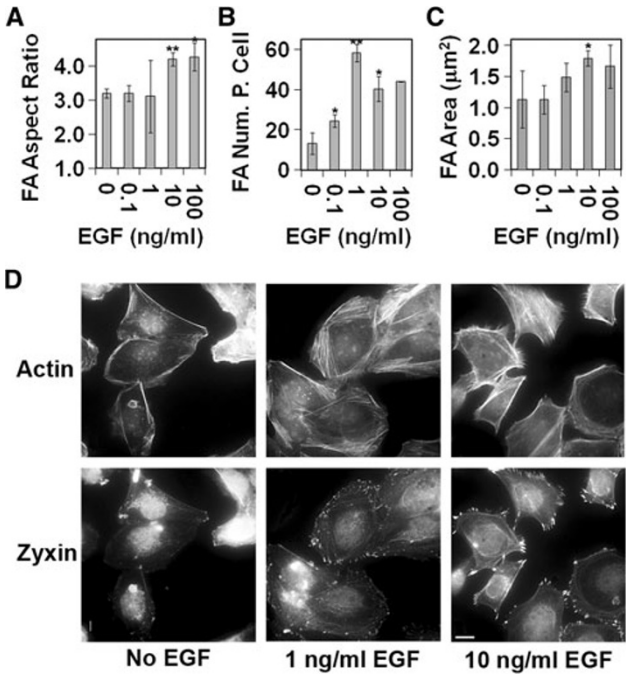

Fig. 3 Focal adhesion growth and actin filament reorganization in A431 cells exposed to soluble EGF. Cells were plated on surfaces modified with 184 pmol/cm^2 RGD. Five hours after cell plating, EGF was added to the medium for 30 min. A separate cell sample was incubated for 5.5 h without EGF, as a control. After 5.5 h, both samples were fixed and stained for zyxin at focal adhesions and for actin filaments. The *graphs* in the *top panel* indicate the 90th percentile of the focal adhesion elongation (**a**), the average number of focal adhesions per cell (**b**), and area (**c**) as a function of EGF concentration. All results are expressed as mean ± confidence intervals (CI). Parameters of FAs in cells that were exposed to soluble EGF and significantly differed from the corresponding parameters of FAs in control cell, not exposed to EGF, at the *P*-value levels $P < 0.05$ and $P < 0.01$ are denoted by one and two *asterisks*, respectively. Fluorescent images of actin- and zyxin-labeled cells exposed to 1 and 10 ng/ml, in comparison to control (no EGF) are presented in the *bottom panel* (**d**). *Scale bar* 15 μm

FA aspect ratio and area (Fig. 3a, c) as well as in the formation of actin cables (Fig. 3d).

Low EGF concentrations, of up to 1 ng/ml, induced a notable increase in the number of elongated FAs (Fig. 3b, d) and actin stress fibers. At higher EGF concentrations (10 and 100 ng/ml), FAs were fewer, larger and more elongated; in many such cells, extensive formation of filopodia, accompanied by extensions of actin-containing microspikes and formation of dense actin stress fibers was seen (Fig. 3d, for 10 ng/ml). The FAs were routinely monitored by zyxin labeling, as focal adhesion marker [42, 43], though essentially the same behavior was observed using paxillin and vinculin labeling (data not shown).

3.3 RGD Density Affects Cell Response to Soluble EGF

To explore the mechanism underlying the effect of EGF on FAs, we systematically modulated both EGF concentration in the medium, and RGD density on the substrate, and examined the cellular responses.

The addition of up to 1 ng/ml soluble EGF to A431 cells, plated on RGD surfaces, led to an increase in the number of FAs per cell (Fig. 4a, b). The number of FAs per cell also increased, with an increase in RGD surface density; this effect was most pronounced at an EGF concentration of 1 ng/ml (Fig. 4a). Cell exposure to higher EGF concentrations, however, (10 and 100 ng/ml EGF) resulted in either cell rounding and detachment from the surface, or in strongly attached cells slightly fewer in total number, but with more elongated FAs. These two scenarios depended on the RGD surface density: at low to intermediate RGD densities, cells rounded and detached from the surface (low bars with dashed border in Fig. 4a) and at high RGD densities, cells remained stable, with slightly more elongated FAs. Interestingly, cells rounded and detached from

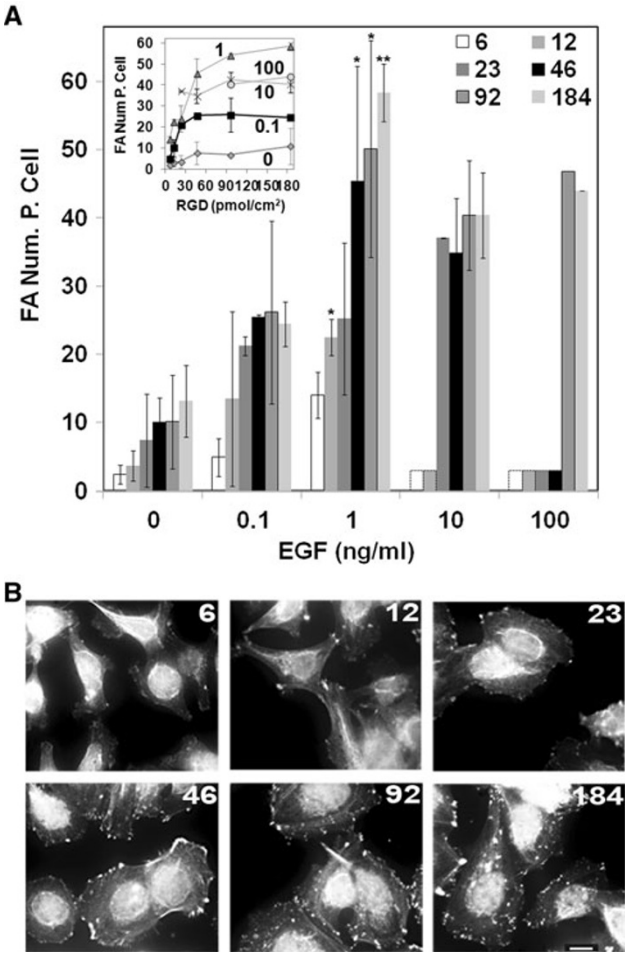

Fig. 4 The effect of RGD density on cell adhesion in response to soluble EGF. Average number of focal adhesions per cell as a function of EGF concentration on surfaces with different RGD densities (**a**), the *numbers* at the *top right* of the *graphs* are the RGD density in pmol/cm^2. *Low bars* with *dashed borders* represent a scenario where cells detached from the surface. The *insert* in **a**, at the *top left* represents the same data as that seen in the main graph, where the average number of focal adhesions per cell are plotted as a function of the surface RGD density. The *numbers* at the *top* of each *graph* represent the applied EGF concentrations in ng/ml. All results are expressed as mean ± confidence intervals (CI). *Number* of FAs in cells plated on 46, 92 and 184 pmol/cm^2 RGD surfaces that were significantly higher than the *number* of FAs in cells plated on both 6 and 12 pmol/cm^2 RGD surfaces at the *P*-value levels $P < 0.05$ and $P < 0.002$ are denoted by *one* and *two asterisks*, respectively. The images in the *bottom panel* are of A431 cells, plated on surfaces modified with RGD at different densities, following stimulation with 1 ng/ml EGF. The *number* on each image indicates the RGD density in pmol/cm^2. The experimental procedure was the same as that described in the legend to Fig. 3. *Scale bar* 15 μm

23 and 46 pmol/cm^2 RGD surfaces, but remained strongly attached to 92 and 184 pmol/cm^2 RGD surfaces, when 100 ng/ml EGF was added, despite the fact that at these RGD densities, cell spreading was quite similar, in the absence of EGF (Fig. 2).

Figure 4a (insert) shows the number of FAs plotted as a function of the surface RGD density. The maximum possible number of FAs per cell is determined by the EGF concentration. This is indicated by the plateau reached at a threshold RGD density of 46 pmol/cm^2 RGD, which was not affected by EGF concentration.

3.4 Cell Adhesion in Response to Global or Local EGF Stimulation

The effect of the mode of receptor stimulation (i.e., global or local) on the synergy between integrin and EGFR was investigated by tracking the cells' adhesive response to surface-bound EGF in comparison to soluble EGF, as a function of the RGD and EGF densities.

Figure 5 indicates that the effect of soluble or immobilized EGF on cell adhesion was significant only at a certain threshold level: At a minimal amount of EGF [$(0.75 \pm 0.28) \times 10^3$ fmol] cells become significantly smaller and more round regardless of whether the EGF was soluble or immobilized (Fig. 5b, c). However, the effect of immobilized EGF on cell adhesion differed greatly from that of soluble EGF above this threshold EGF amount: Cells were plated on RGD surfaces and 21.4 ± 5.3 pmol/cm^2 [$(4.19 \pm 1.04) \times 10^3$ fmol] immobilized EGF displayed a significant increase in the number of FAs per cell and in cell spreading (with the projected cell area returning to the same value as that seen in the absence of EGF; for non- treated cells) (Fig. 5a, b). In contrast, cells plated on RGD-only surfaces, exposed to the same level of EGF in soluble form, showed only a slight increase in the number of FAs per cell and a further reduction in cell spreading (Fig. 5a, b). A further increase in the level of immobilized EGF resulted in loss of FAs and cell detachment. However, treatment with the same level of soluble EGF did not lead to cell detachment; indeed, some FAs remained (Fig. 5a, d). With both forms of stimulation, FAs became more elongated as EGF levels increased, while cells became more round (Fig. 5d).

The immobilization of EGF also had a profound effect on the arrangement and density of actin stress fibers. Cells that spread on 46 pmol/cm^2 RGD surfaces in the absence of EGF displayed actin stress fibers at the cell periphery, and only a few filopodia. As EGF levels increased, more actin stress fibers across the cell were observed, accompanied by an increase in filopodia and actin-containing microspikes (Fig. 5d). The increase in actin stress fibers and actin-containing filopodia and microspikes was by far more significant at the immobilized-EGF density (21.4 ± 5.3 pmol/cm^2 or $(4.19 \pm 1.04) \times 10^3$ fmol) than at the same level of soluble EGF. In addition, cells plated on immobilized EGF at this density adopted a large, pancake-like shape with extended lamellipodia containing

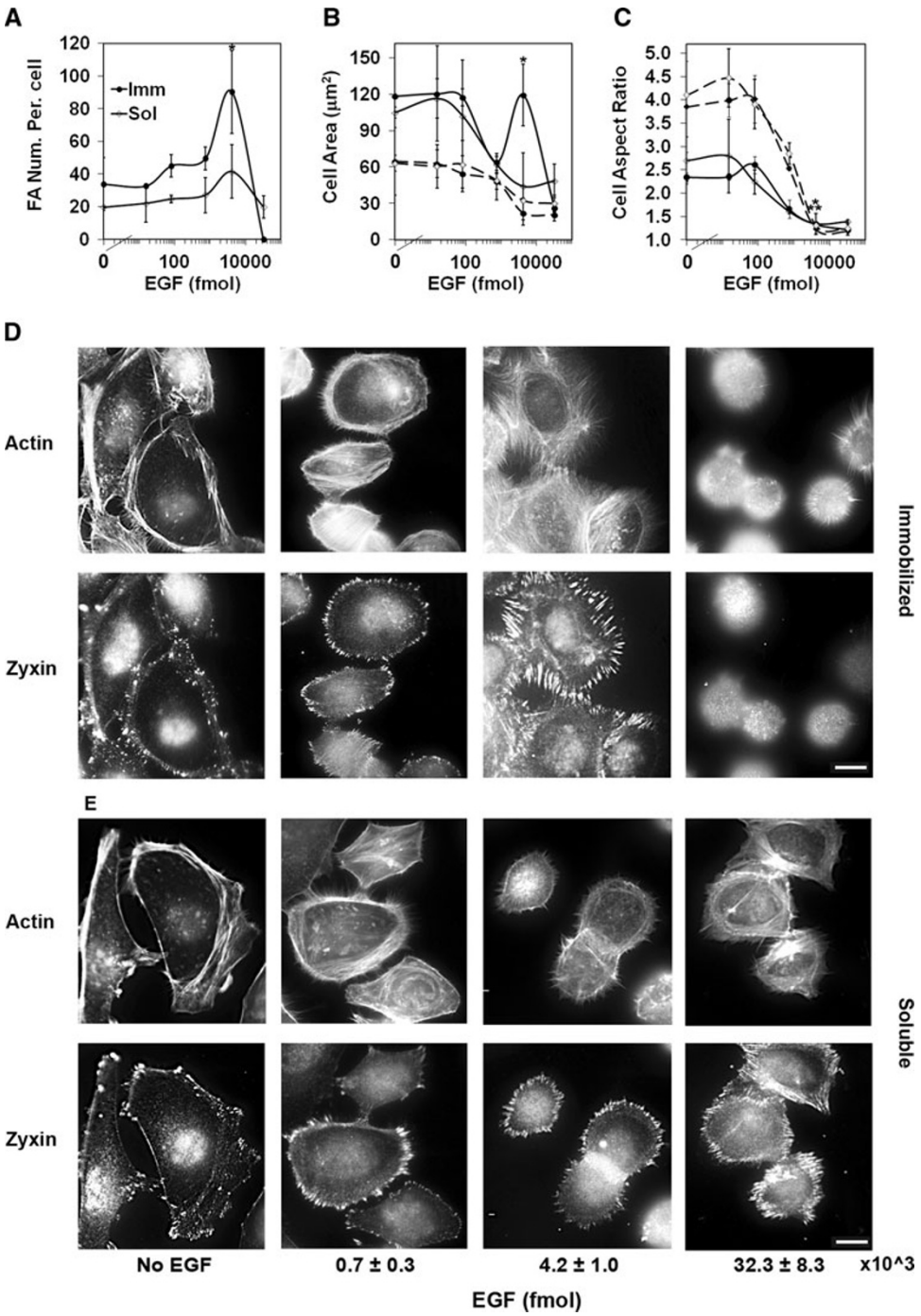

Fig. 5 A comparison between cell response to immobilized and soluble EGF as a function of RGD density and total EGF amounts. For comparison, the amounts of immobilized and soluble EGF are calculated for the given well area or the given volume, respectively. The 70th percentile of the cell area (**b**) and cell aspect ratio (**c**) are summarized for cells plated on either 12 (*dashed line*) or 46 (*solid line*) pmol/cm^2 RGD-modified surfaces as a function of the amount of immobilized (Imm *dark circles*) or soluble (Sol *empty diamond*) EGF. The average numbers of focal adhesions per cell as a function of EGF are presented for cells plated on 46 pmol/cm^2 RGD surfaces (**a**). All results are expressed as mean ± confidence intervals (CI). Number of FAs per cell or cell area for cells plated on 46 pmol/cm^2 RGD surfaces and $(4.19 \pm 1.04) \times 10^3$ fmol immobilized EGF that were significantly different from the same parameters of cells exposed to the same amount of soluble EGF at the *P*-value level $P < 0.05$ are denoted by *one asterisks*. This *mark* also indicate the *P* value level for the differences between the parameters of cells plated on $(0.75 \pm 0.28) \times 10^3$ and $(4.19 \pm 1.04) \times 10^3$ fmol immobilized EGF. Aspect ratio of cells plated on 12 or 46 pmol/cm^2 RGD surfaces and $(4.19 \pm 1.04) \times 10^3$ fmol immobilized EGF differed from cells plated on RGD only surfaces at a *P*-value of $P < 0.05$ (*) and $P < 0.01$ (**), respectively. *Bottom panel* images of zyxin- and actin-labeled A431 cells, plated on surfaces modified with 46 pmol/cm^2 RGD and various amounts of immobilized (**d**) or soluble EGF (**e**). Cells were incubated on the different surfaces for 5 h, and then fixed and stained for zyxin and actin. *Scale bar* 15 μm

short stress fibers, probably responsible for the marked increase in cell area.

The difference between stimulation with soluble and immobilized EGF was also RGD density-dependent: the differences in cell spreading above a critical EGF level were observed only on surfaces with high RGD densities (23 and 46 pmol/cm^2 RGD), but not on surfaces with low RGD densities (6 and 12 pmol/cm^2 RGD; data for 6 and 23 pmol/cm^2 RGD is not shown, and data for 12 and 46 pmol/cm^2 RGD is shown in Fig. 5b, c). Cell response to soluble or immobilized EGF was the same for all levels of EGF on low density, 12 pmol/cm^2, RGD surfaces. At the critical EGF level, the cells became smaller, rounder, and with increasing EGF levels, detached from the surface.

3.5 Discussion

3.5.1 Cross-Talk Between RGD and EGF in the Modulation of Cell Adhesion

Silane-PEG-biotin- modified surfaces enabled the selective conjugation of biotinylated RGD and EGF molecules at a controlled orientation, and with good accessibility, while preventing non-specific binding of proteins from the extracellular environment, and non-specific cell adhesion. The densities obtained for surface-immobilized biotinylated EGF were within the same range of densities published in the literature for other EGF immobilization techniques [17, 18, 24, 44].

Cell adhesion experiments indicate that stimulation of serum-starved A431 cells with EGF led to the formation of FAs, in combination with cortical and cell-crossing actin stress fibers, extensive filopodia, and actin-containing microspikes. These EGF-mediated cell adhesion responses were found to be RGD- and EGF density- or EGF concentration-dependent (Figs. 3, 4, 5): EGF acted as an adhesion stimulator up to a certain threshold level, above which it behaved as an adhesion suppressor. This held true for both immobilized and soluble EGF, and was highly dependent on the RGD surface density (Figs. 4, 5).

It has been reported that intercellular contractile forces are generated following EGF stimulation, through the activation of myosin light chain (MLC; a subunit of myosin II motor protein) promoting actin-myosin interaction either through ERK/MAPK [6, 8] or through the activation of PLCγ [45] signaling pathways. Thus, the observed increase in FA size and number may be required to sustain the intercellular forces generated by EGF stimulation. Cells plated on surfaces with low to medium densities of RGD and treated with high amounts of EGF cannot sustain these contractile forces, due to their lack of strong cell-surface contact points; hence, their FAs disassemble, they round up and detach from the surface.

The effect of EGF on the sensitivity of cell-adhesion responses to RGD density is summarized in Figs. 2 and 4. In the absence of EGF, cell spreading showed only minimal changes in response to RGD densities above 23 pmol/cm^2 (Fig. 2). However, a significant increase in the number of FAs was observed in response to 1 ng/ml EGF, as the RGD density was increased from 6 to 184 pmol/cm^2 (Fig. 4). Moreover, cells remained attached to 23, 46, 92 and 184 pmol/cm^2 RGD surfaces upon stimulation with 10 ng/ml EGF, but when stimulated with 100 ng/ml EGF, only cells plated on 92 and 184 pmol/cm^2 RGD surfaces remained (Fig. 4). This indicates that the minimum RGD density required for complete cell spreading in the absence of EGF is lower than that required for the formation of stable cell–matrix contacts following EGF stimulation.

3.5.2 Soluble Versus Immobilized EGF Stimulation

Our results show that the cell adhesion response to EGFR stimulation is significant only at a critical EGF level, above which cellular response to immobilized (local) EGF is more pronounced than to soluble (global) stimulation. The following section addresses the possible reasons for this behavior.

Presentation of a ligand on a surface, such as that coated with immobilized EGF, introduces better control over ligand conformation, availability and density. Cell stimulation with soluble ligands is dependent on the diffusion potential of the ligand, and the probability that it reaches the receptor in the appropriate conformation. Hence, stimulation with immobilized ligands may be more effective.

In addition, the binding of soluble EGF to EGFR under physiological conditions is accompanied by the internalization of the EGFR-EGF complex. This mechanism is used by the cell to regulate EGF stimulation [46]. However, the complex formed between an EGFR and immobilized EGF cannot be internalized, thereby inducing ongoing cell stimulation [47, 48], which may lead to constant, long-lasting cellular contractile forces (see third paragraph of the "3.5"). Our results may imply that, at the EGF level, at which the cells are near the point of detachment, higher numbers of FAs with greater aspect ratios are needed to balance these contractile forces, than are needed to balance potentially intermittent contractile forces induced by soluble EGF. This view is supported by the observed cytoskeletal changes, which are also consistent with an additional response to force. At a still higher immobilized-EGF density, cells can no longer withstand these contractile forces, and they detach from the surface.

Still, a question remains regarding the presence of a specific critical EGF threshold level, which induces significant changes in cell adhesion behaviors. This can be

explained in terms of the lateral EGF–EGF distance in an EGFR dimer. According to crystal structure analysis, the distance between EGF molecules in dimerized doubly occupied EGFRs is 7.9 nm [49]. EGFR dimerization under physiological conditions follows the binding of EGF to its receptor, concomitant with the receptor's transformation from an inactive monomeric form to an active homodimer form, leading to the initiation of the EGF signaling cascade [18–20]. Low–EGF density surfaces correspond to average EGF–EGF spacings, which are 3–7 times larger than that of EGF molecules in doubly EGF-occupied EGFRs dimer, hence in most cases would not induce EGFRs dimerization. However, at the observed critical EGF surface density 3.8 ± 1.4 pmol/cm^2 [$(0.75 \pm 0.28) \times 10^3$ fmol], the average spacing between each EGF molecule on the surface is 6.8 ± 1.1 nm, enabling and maybe even forcing EGF-occupied, monomeric EGFR to dimerize. This may be the reason for the significant reduction in cell area and polarity at the critical EGF density. Above the critical density, at the same range of EGF–EGF spacing at a doubly EGF- occupied EGFRs dimer, cellular response to immobilized- EGF become by far more profound than that obtained by soluble EGF, as manifested by the significant increase in both the number of FAs per cell and in cell spreading which was not observed upon stimulation with the same level of soluble EGF (Fig. 5a, b). We note that the values calculated for the spacings between the immobilized EGF molecules are average values; a more precise assessment of the effect of EGF spacing on the EGF-mediated adhesion response could be achieved with hexagonally nanopatterned surfaces displaying a homogeneous ligand distribution [1].

The co-immobilization of both EGF and RGD onto the same surface potentially leads to the aggregation of EGFRs in close proximity to integrins, and may thus enhance EGFR-integrin cooperativity. The critical density of immobilized EGF lies within the range of the RGD density, suggesting a role for EGFR-integrin cooperativity in EGF- mediated adhesion response. It has been suggested that co-clustering of EGFR and integrins constitutes a prerequisite for the co-clustering and synergism of downstream signaling molecules [50, 51]. The enhanced effect of immobilized EGF on cell adhesion, compared to soluble EGF at these small ratios between integrin and EGFR ligand densities, may imply that close proximity is a requirement for direct integrin-EGFR cooperativity. Ligand-mediated, activated integrin and EGFR have been shown to cooperate through Src, inducing the activation of Rac1 and the suppression of RhoA activity [16, 52, 53]. Rac1 activation results in lamellipodia and filopodia formation, leading to cell spreading, and has also been shown to precede cell detachment following FA disassembly [52].

4 Summary and Conclusions

We have shown that there is a synergism in the cell adhesion response between integrin and EGFR, in an RGD- and EGF density- or concentration-dependent manner. Cell stimulation with low to intermediate doses of EGF induces adhesion activation, whereas high EGF doses suppress adhesion. The effect of immobilized EGF differs from the effect of soluble EGF above a certain EGF density. This may be because surface presentation of the EGF ligand enables (1) more precise control over ligand accessibility and density; (2) the non-internalization of the receptor-ligand complex, hence resulting in constant, ongoing cellular stimulation; (3) the close proximity of the EGF and RGD ligands, which may "force" the integrins and EGFRs to aggregate. The critical EGF density is the one most likely required for the induction of EGFR dimerization, and lies within the range of the RGD density, suggesting a role for EGFR-integrin cooperativity in EGF- mediated adhesion response.

Acknowledgments This study was supported by the European Union Seventh Framework Programme (FP7/2007-2013)), under grant agreement no NMP4-LA-2009-229289 NanoII, and Grant agreement no NMP3-SL-2009-229294 NanoCARD (*to B. G. and J. S.*) and by the *National Institutes of Health (NIH) Common Fund Nanomedicine Program* (*PN2 EY016586*) (*to B.G.*) *and DFG project, DFG Gz: SP 520/13-1* (*to J.S.*). We wish to thank Prof. Zvi Kam and Yuvalal Liron for their expert help with image analysis and advanced microscopy. We would like to acknowledge Dr. Bilha Schechter for her help in producing the radioactive ^{125}I-EGF, and Dr. Hagai Cohen for the XPS analysis. B. G. is the incumbent of the Erwin Neter Professorial Chair in Cell and Tumor Biology. J. S. is a Weston Visiting Professor at the Weizmann Institute of Science, Israel.

References

1. Cavalcanti-Adam EA, Volberg T, Micoulet A, Kessler H, Geiger B, Spatz JP (2007) Biophys J 92(8):2964–2974
2. Miyamoto S, Teramoto H, Gutkind JS, Yamada KM (1996) J Cell Biol 135(6):1633–1642
3. Are A, Pinaev G, Burova E, Lindberg U (2001) Cell Motil Cytoskeleton 48(1):24–36
4. Genersch E, Schuppan D, Lichtner RB (1996) J Mol Med 74(10):609–616
5. Pichard V, Honore S, Kovacic H, Li CG, Prevot C, Briand C, Rognoni JB (2001) Histochem Cell Biol 116(4):337–348
6. Cheresh DA, Leng J, Klemke RL (1999) J Cell Biol 146(5):1107–1116
7. Ridley AJ, Paterson HF, Johnston CL, Diekmann D, Hall A (1992) Cell 70(3):401–410
8. Xie H, Pallero MA, Gupta K, Chang P, Ware MF, Witke W, Kwiatkowski DJ, Lauffenburger DA, Murphy-Ullrich JE, Wells A (1998) J Cell Sci 111:615–624

9. Schlessinger J, Geiger B (1981) Exp Cell Res 134(2):273–279
10. Toral C, Solano-Agama C, Reyes-Marquez B, Sabanero M, Talamas P, del Pliego MG, Mendoza-Garrido ME (2007) Cell Tissue Res 327(1):143–153
11. Marcoux N, Vuori K (2005) Cell Signal 17(11):1449–1455
12. Miyamoto S, Teramoto H, Coso OA, Gutkind JS, Burbelo PD, Akiyama SK, Yamada KM (1995) J Cell Biol 131(3):791–805
13. Cluzel C, Saltel F, Lussi J, Paulhe F, Imhof BA, Wehrle-Haller B (2005) J Cell Biol 171(2):383–392
14. Geiger B, Bershadsky A, Pankov R, Yamada KM (2001) Nat Rev Mol Cell Biol 2(11):793–805
15. Miyamoto S, Akiyama SK, Yamada KM (1995) Science 267(5199):883–885
16. Moro L, Venturino M, Bozzo C, Silengo L, Altruda F, Beguinot L, Tarone G, Defilippi P (1998) EMBO J 17(22):6622–6632
17. Nakaji-Hirabayashi T, Kato K, Iwata H (2009) Bioconjug Chem 20(1):102–110
18. Ichinose J, Morimatsu M, Yanagida T, Sako Y (2006) Biomaterials 27(18):3343–3350
19. Schlessinger J (2002) Cell 110(6):669–672
20. Lemmon MA, Bu ZM, Ladbury JE, Zhou M, Pinchasi D, Lax I, Engelman DM, Schlessinger J (1997) EMBO J 16(2):281–294
21. Schumann K, Lammermann T, Bruckner M, Legler DF, Polleux J, Spatz JP, Schuler G, Forster R, Lutz MB, Sorokin L, Sixt M (2010) Cell 32:703–713
22. Fan VH, Au A, Tamama K, Littrell R, Richardson LB, Wright JW, Wells A, Griffith LG (2007) Stem Cells 25(5):1241–1251
23. Chen GP, Ito YY (2001) Biomaterials 22(18):2453–2457
24. Ito Y, Chen GP, Imanishi Y, Morooka T, Nishida E, Okabayashi Y, Kasuga M (2001) J Biochem (Tokyo) 129(5):733–737
25. Maheshwari G, Wells A, Griffith LG, Lauffenburger DA (1999) Biophys J 76(5):2814–2823
26. Maheshwari G, Brown G, Lauffenburger DA, Wells A, Griffith LG (2000) J Cell Sci 113(10):1677–1686
27. Elloumi I, Kobayashi R, Funabashi H, Mie M, Kobatake E (2006) Biomaterials 27(18):3451–3458
28. Langer R (2009) Adv Mater 21(32–33):3235–3236
29. Dunlop IE, Zorn S, Richter G, Srot V, Kelsch M, van Aken PA, Skoda M, Gerlach A, Spatz JP, Schreiber F (2009) Thin Solid Films 517(6):2048–2054
30. Wells A, Ware MF, Allen FD, Lauffenburger DA (1999) Cell Motil Cytoskeleton 44(4):227–233
31. Wells A (1999) Int J Biochem Cell Biol 31(6):637–643
32. Jo S, Park K (2000) Biomaterials 21(6):605–616
33. Hyre DE, Le Trong I, Merritt EA, Eccleston JF, Green NM, Stenkamp RE, Stayton PS (2006) Protein Sci 15(3):459–467
34. Huang NP, Voros J, De Paul SM, Textor M, Spencer ND (2002) Langmuir 18(1):220–230
35. Gunawan RC, King JA, Lee BP, Messersmith PB, Miller WM (2007) Langmuir 23(21):10635–10643
36. Amirgoulova EV, Groll J, Heyes CD, Ameringer T, Rocker C, Moller M, Nienhaus GU (2004) Chem Phys Chem 5(4):552–555
37. Jang Y, Oh SY, Park J-K (2006) Enzyme Microb Technol 39(5):1122–1127
38. Hoffman LM, Jensen CC, Kloeker S, Wang CLA, Yoshigi M, Beckerle MC (2006) J Cell Biol 172(5):771–782
39. Paran Y, Ilan M, Kashman Y, Goldstein S, Liron Y, Geiger B, Kam Z (2007) J Struct Biol 158(2):233–243
40. Zamir E, Katz BZ, Aota S, Yamada KM, Geiger B, Kam Z (1999) J Cell Sci 112(11):1655–1669
41. Kam Z, Zamir E, Geiger B (2001) Trends Cell Biol 11(8):329–334
42. Zaidel-Bar R, Ballestrem C, Kam Z, Geiger B (2003) J Cell Sci 116(22):4605–4613
43. Crawford AW, Beckerle MC (1991) J Biol Chem 266(9):5847–5853
44. Goncalves R, Lopes Martins MC, Oliveira MJ, Almeida-Porada G, Barbosa MA et al (2010) J Biomed Mater Res Part A 94A(2):576–585
45. Iwabu A, Smith K, Allen FD, Lauffenburger DA, Wells A (2004) J Biol Chem 279(15):14551–14560
46. Mosesson Y, Mills GB, Yarden Y (2008) Nat Rev Cancer 8(11):835–850
47. Chen GP, Ito Y, Imanishi Y (1997) Biochim Biophy Acta Mol Cell Res 1358(2):200–208
48. Ito Y (1998) Nanotechnology 9(3):200–204
49. Ogiso H, Ishitani R, Nureki O, Fukai S, Yamanaka M, Kim JH, Saito K, Sakamoto A, Inoue M, Shirouzu M, Yokoyama S (2002) Cell 110(6):775–787
50. Yamada KM, Miyamoto S (1995) Curr Opin Cell Biol 7(5):681–689
51. Schwartz MA, Baron V (1999) Curr Opin Cell Biol 11(2):197–202
52. Brunton VG, MacPherson IRJ, Frame MC (2004) Biochim Biophys Acta Mol Cell Res 1692(2–3):121–144
53. Huveneers S, Danen EHJ (2009) J Cell Sci 122(8):1059–1069